Actual achievements and future challenges of HPFRC for structural rehabilitation of bridges

Adriano Reggia[1,*], *Ivan* Trabucchi[1], *Alessandro* Morbi[2] and *Giovanni* A. Plizzari[1]

[1] University of Brescia, Brescia, Italy
[2] Italcementi S.p.A., Bergamo, Italy

Abstract. The state of road infrastructures in many advanced countries is rapidly changing under the impulse of massive funding from governments, eager to have more efficient and safer transportation systems. The use of well-known materials such as fibre-reinforced concrete (FRC) is finding a growing space for structural rehabilitation of bridges; the adopted material is often defined as High performance fibre reinforced concrete (HPFRC) due to its enhanced performance. The paper presents the principal findings of an EU-funded project that involved the repair of two road bridges in Italy using HPFRC. The project has successfully carried out the jacketing of bridge piers and cap-beams, heavily damaged by corrosion, with a new HPFRC layer of reduced thickness (40-60 mm) and limited use of steel reinforcements. Experimental tests carried out in the laboratory of the University of Brescia on 1:2 scaled specimens have shown the possibility to increase the load bearing capacity of the cap beams (with respect to vertical loading) up to 73%, with moderate effects on the change in stiffness and ductility of the existing structure. Based on field and laboratory experience, the article eventually presents some new challenges for the use of HPFRC in the reduction of environmental impact of construction industry.

1 Introduction

The number of bridges showing signs of inadequacy to the new traffic demands is constantly growing. This is mainly due to the deterioration of the infrastructures, primarily related to corrosion [1, 2, 3] and to the increase of vehicle weight and number.

In addition to the natural deterioration of construction materials due to the aggressiveness of the environment and a greater awareness of the seismic risk in many countries [4, 5], now described in structural codes (but not present at the time of construction), one of the main causes of bridge degradation is represented by use of de-icing salts, which favours the corrosion of the reinforcement of decks and of structures underneath [6, 7, 8, 9].

Some design choices commonly adopted a few decades ago, including the emblematic case of dapped-end girders, are now considered critical for structural durability and, therefore, for the residual bearing capacity of the bridges.

In this critical context, demonstrated by some bridge collapses occurred all over the world during the last few years, a traffic monitoring plan on the road network and on bridges has now become an urgent need for the road administrations, in order to meet the requirements of safety and efficiency of road transportation. In particular, it is necessary to have a detailed picture of the actual performance, both for bridges and roads, to monitor and regulate traffic on the basis of the safety of existing bridges, especially in the main road networks [10]. It is also necessary to properly control overloads and undesired dynamic effects [11] in critical bridges, in order to limit bridge degradation and to intervene with bridge repairing/retrofitting, where necessary. The only alternative is often the bridge demolition and replacement that is not always possible and may have heavy social and economic impact.

Concrete bridge repairing and retrofitting can be achieved with the use of new materials and technologies now available on the market [12], much more effective than traditional ones and nowadays often codified by current building codes.

High performance fibre reinforced concretes (HPFRCs) represent a promising material for the retrofitting of existing bridge elements (*i.e.* piers and decks). HPFRCs are made by the combination of a cementitious matrix and fibres, which lead to a material with low permeability and high strength (*i.e.* in compression and in tension, both before and after cracking, when the resistance is provided by the bridging effect of fibres).

The paper presents a real repair intervention on two bridges in the north of Italy (Province of Brescia) subject to a severe state of corrosion of the piers that were retrofitted with HPFRC. In particular, the paper illustrates the case study and the experimental tests carried out at the laboratory of the University of Brescia to characterize the behaviour of the cap beam before and

* Corresponding author: adriano.reggia@unibs.it

after reinforcement with HPFRC, with and without without additional reinforcements.

2 Case study

2.1 In situ operations

The experimental campaign have been carried out on specimens whose geometry has been obtained from two (twin) existing bridges located in the Province of Brescia in Lombardy, Italy. The bridges were retrofitted by the Province of Brescia in 2020/2021, as part of the Sustainable and Resilient Mobility (MoSoRe) project. The intervention pursues the objectives and intentions stated by the Regional Strategy for Sustainable Development, approved by Region Lombardia in the field of infrastructure.

The bridge has three spans of approximately 900 cm with multiple column piers and cap beam, Fig. 1. The abutments were built with beams resting on reinforced concrete piles, which penetrate the ground more than six meters. Each pier consists of a frame of four columns with a span of 327 cm (from the vertical axis of two consecutive columns). Each column has a rectangular cross-section 41 cm wide and 90 cm deep, and is reinforced by 14Ø16 longitudinal steel rebars and Ø10 stirrups with a 20 cm spacing. The foundation is a beam 120 cm wide and 90 cm deep, reinforced with 12Ø16 longitudinal rebars. The transverse reinforcement consists of 2Ø12 deformed bars at 20 cm spacing. At the top of the pillars there is the cap beam, with a total length of 1132 cm; it extends beyond the pillars by about 55 cm. Its section is rectangular with a base of 90 cm and a height of 80 cm. The cap beam is reinforced by 7Ø22 longitudinal rebars, both at the top and the bottom, while at the middle height there are 2Ø12. Shear reinforcement consists of 2Ø16 deformed bars every 20 cm, lapped on the side of the beam (unconventional detailing). All these structural elements have a net concrete cover of about 2 cm. Steel rebars are made with FeB44k steel (yielding tension of 430 MPa), very similar to B450C steel available in Italy nowadays. Concrete has a mean cubic compressive strength of 31 MPa.

The piers were in an advanced state of material degradation. In particular, the continuous flow of rainwater and chemicals (de-icing salts used during winter season) penetrating into the joints of the deck (without waterproofing systems) caused concrete deterioration and corrosion of reinforcements. This phenomenon was more evident on the cap beam and on the header columns, where longitudinal bars and transverse reinforcements were exposed to the weather (due to concrete spalling). Aside from material degradation phenomena, the piers and deck do not show relevant structural problems and their crack patterns were not considered significant.

The retrofitting mainly involved the piers. Initially, the existing concrete cover on the piers, showing signs of deterioration, was removed. After the demolition of concrete, new longitudinal and transverse reinforcements were placed around the columns and beams. Columns were reinforced with eight Ø16 longitudinal bars and Ø12 stirrups every 200 mm. The beams were reinforced with 4Ø20 top and bottom longitudinal bars. The supplementary reinforcements added to the cap beam were Ø16 deformed bars spaced 20 cm. A new layer of HPFRC was cast around the existing elements (*i.e.* jacketing) with a thickness ranging between 4 and 6 cm. The HPFRC had a strength class C70/85 and a toughness class 6b, according to fib Model Code 2010 [13]. Additional reinforcements were made with B450C steel (yielding tension of 450 MPa). In addition, the intervention was completed with the revamping of the transversal joints of the decks, the replacement of road safety barriers and asphalting.

Fig. 1. Existing bridge adopted as case study for the experimental campaign.

2.2 Specimen geometry

The present work focuses its attention on the most damaged structural element of the frame piers of the bridge: the cap beam. Six scaled specimens (1:2) were realized with the aim of better understanding the structural capacity of such beams before and after the repair, with particular emphasis on their behaviour under vertical (traffic) loads. Within this experimental campaign, these specimens were grouped in three classes: the first group of two beams (Reference) represented the beam before repair; the second group of two beams (Reinforced#01) represented the beam in its final state after jacketing (as realized on the field); the third group (Reinforced#02) represented a simplified layout of the repair in which HPFRC is applied without additional reinforcements, Fig. 2. Table 1 shows the geometrical features of the specimens with respect to the full-size beams. Details of specimens and reinforcement layouts are given in Fig. 3.

Even though on the real structural elements the load is applied as a distributed load (through the deck of the bridge itself) on a continuous beam, the experimental tests were performed considering a concentrated load applied in the centre of a simply supported beam. This simplification allows a significant facilitation in the execution of the tests without compromising its scientific relevance. On the other hand, considering a concentrated load instead of a distributed load is a more unfavourable

condition for the beam and, therefore, more significant for characterising its behaviour.

(a)

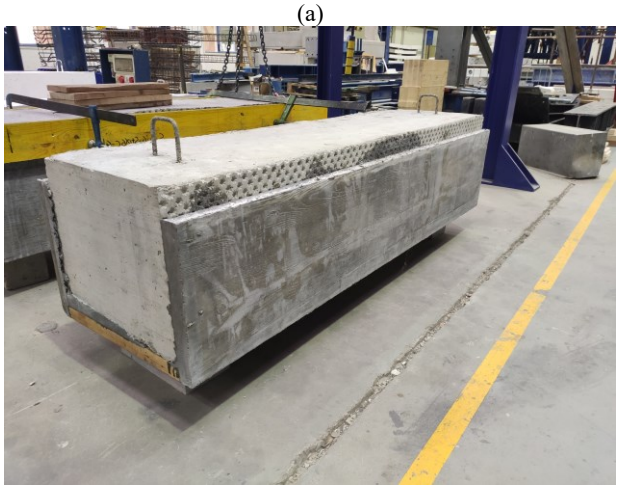

(b)

Fig. 2. Reinforced#02: (a) specimen before casting with highlighted on the right the HPFRC layer after casting and (b) reinforced specimen after demoulding.

Table 1. Geometrical features of the specimens with respect to the full-size beams.

		Full-size	Specimen
Side	[cm]	90	45
Height	[cm]	80	40
Span	[cm]	327	164
Top reinfo.	[-]	7Ø22	6Ø12
Mid reinfo.	[-]	2Ø12	2Ø6
Bottom reinfo.	[-]	7Ø22	6Ø12
Stirrups	[-]	(1 +1)Ø16 @20 cm	(1 +1)Ø8 @10 cm
Effective depth	[cm]	75.4	36.7

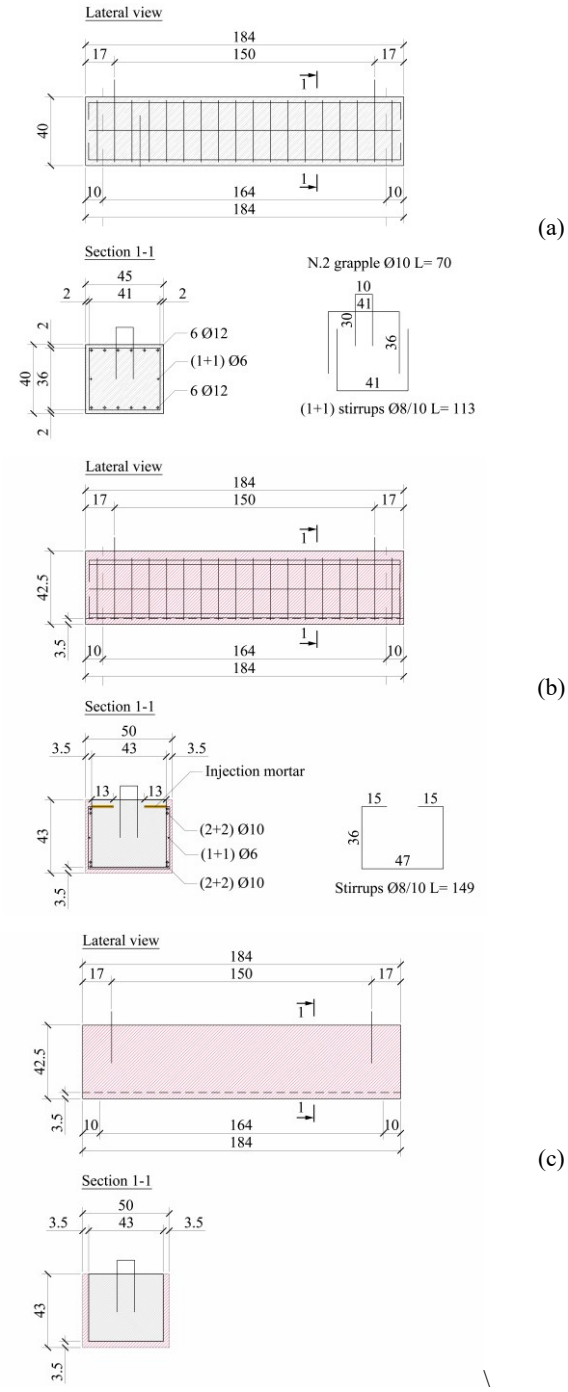

Fig. 3. Specimen details: (a) Reference, (b) Reinforced#01 and (c) Reinforced#02 (dimensions in cm).

2.3 Structural behaviour

The structural behaviour of these specimens can be roughly evaluated considering their shear span/effective depth (a/d) ratio, which is equal to 2.23 (82/36.7). They fall exactly within the "valley of diagonal failure" [14] of the Leonhardt and Walter diagram for beams dominated by strut-and-tie resistance mechanism. It has to be mentioned that, contrary to what has been done within this work, the experiments conducted by Leonhardt and Walter [14] (and later also by Kani [15]) were performed on beams without shear reinforcement. However, the shear design with stirrups having lateral overlap

combined with the degradation of the structure makes this shear reinforcement less effective. Hence, another aim of this study concerns the influence of the stirrups overlap on the shear capacity of the beam.

3 Experimental program

3.1 Test set-up and instrumentation

The test specimen (1 in Fig. 4) was a simply supported beam with steel restraints: a hinge at left (2) and a support at right (3). The beam was tested in flexure with a three point bending test set-up. Mid-span vertical displacement (*i.e.* deflection) was increased by an electro-mechanical actuator (4) up to the failure of the element. The vertical load was applied to the reinforced concrete (RC) beam by means of a steel beam (2 UPN400 made of S235 steel) placed at the centre of the span (5). The steel beam was connected to the electro-mechanical jack by means of a couple of high strength steel bars (6). The electro-mechanical jack was secured to the Laboratory's strong floor (7), thus creating a self-balanced testing system. The load acting on each vertical bar was measured by means of two load cells (13) placed over the steel beam.

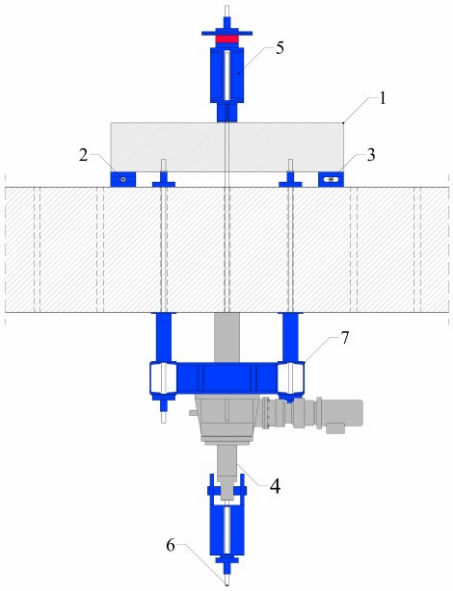

Fig. 4. Experimental test set-up.

Different types of measuring devices were used, as summarized in the following:

- Linear variable displacement transducers (LVDTs) were used to measure the deflection at mid-span and vertical displacements of supports (on both sides of the beam).
- Linear potentiometers (LPs) were used to measure either compressive or tensile deformations of the specimen at the midspan and near the ends of the beams.
- Strain gauges (SGs) were used to measure shear reinforcements strains. They were applied directly to the steel bars and protected by the surrounding concrete during the test.
- Embedded strain gauges (ESGs) were adopted to evaluate the deformation of HPFRC jacketing into which they were immersed.

The displacement gauges are presented in Fig. 5: it includes six inductive displacement transducers (LVDTs) and eight potentiometric transducers (LPs). In particular, two LPs (LP1 and LP2) were used to measure the shortening developed along the compressed struts of the beams, considering an inclinations of about 26°; two LPs (LP5 and LP6) were used to catch the possible formation of a major shear crack; four LPs (LP7-LP10) were used to measure longitudinal deformations at the edges of the cross-section of the beam at the mid-span. For the reinforced samples other transducers were used: three LVDTs (LVDT7-LVDT9) to measure possible detachments of HPFRC jacketing and four ESGs (ESG1-ESG4) to measure HPFRC jacketing deformation.

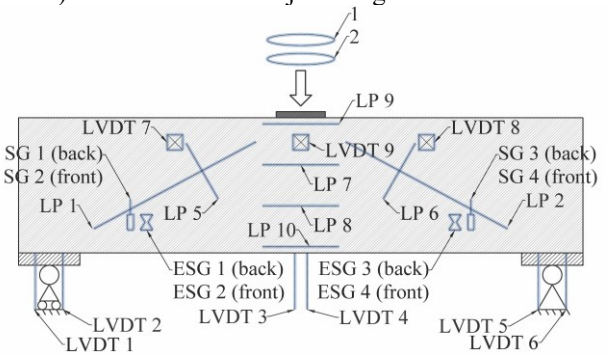

Fig. 5. Side view of the specimen with the adopted instrumentation.

Digital image correlation (DIC) was extensively used in the experimental campaign to evaluate the deformations and displacements of the specimens during testing. It was applied to an entire side of each beam with the aim of providing a significant increase in the quality of the information on the development of deformations and the crack pattern of the beams. The DIC measurements were validated by the measurements from the displacement gauges. DIC made a great contribution to the construction of the crack pattern of the specimens, especially for the reinforced specimens, for which the microcracking was not visible to the naked eye.

The photographic instrumentation employed consisted of two digital cameras, positioned on the side opposite the one with the traditional instrumentation. A photograph was taken every 30 seconds and, at the end of the test, all photograps were transferred to GOM Correlate software. The software has advanced algorithms to perform DIC and point tracking, allowing coordinates to be measured with sub-pixel accuracy.

3.2 Materials

In the following, the results of the mechanical characterisation of the materials will be given. The results obtained for the reinforcements, including both longitudinal bars and stirrups, will first be discussed, and

then the characteristics of Normal Strength Concrete (NSC) and HPFRC will be presented.

Mechanical properties of steel reinforcements were measured according to EN 15630-1 [16]. Four different steel diameters were used in the experimental campaign, namely Ø6, Ø8, Ø10 and Ø12. The results of tensile tests are presented in Table 2, where f_y and f_t represents the average yield and ultimate strength, respectively; Coefficient of Variations (CoVs) are provided in brackets.

Table 2. Mechanical properties of steel reinforcements.

Bar diameter [mm]	f_y [MPa]	f_t [MPa]
6	594.8 (0.02)	610.2 (0.02)
8	547.0 (0.01)	658.6 (0.01)
10	544.7 (0.01)	665.9 (0.01)
12	532.1 (0.01)	648.5 (0.01)

NSC is used for the construction of Reference, Reinforced#01 and Reinforced#02 beams. Mechanical characterization was performed using cubes and cylinders whose dimensions comply with the specifications of EN 12390-1 [17]: cubes having a side of 150 mm and cylinders having a diameter of 100 mm and a height of 200 mm. Specimens were cured under controlled conditions according to the indications provided by the EN 12390-2 [18] standard, *i.e.* by placing the cubes and cylinders in a climatic chamber at 20±2°C with relative humidity ≥95% up to 24 hours before the test. The compression tests were carried out at different ages to evaluate the evolution of the resistance over time, in accordance with the provisions of the EN 12390-3 standard [19]. The mean value of cubic compressive strength at 28 days, $f_{cm,cube}$, was equal to 34.0 MPa with a CoV equal to 0.11. Secant modulus of elasticity was measured in accordance with EN 12390-13 [20]; for this purpose cylindrical specimens were used. The mean value of the modulus of elasticity, E_{cm}, was equal to 39672 MPa with a CoV of 0.09.

HPFRC was used for the jacketing of Reinforced#01 and Reinforced#02 beams. The tests were carried out on cubes, cylinders and beams whose dimensions comply with EN 12390-1 [17]. Also in this case, curing took place in a controlled climatic chamber as specified by EN 12390-2 [18]. The compression tests were carried out on HPFRC cubes in accordance to EN 12390-3 [19] at different ages. The elastic modulus was measured in accordance with EN 12390-13 [20] and the values are presented in Table 3. The mechanical characterization of HPFRC in flexure was carried out according to EN 14651 [21] standard. The tests were carried out on 150×150×600 mm notched beams with a three point bending test set-up. A hydraulically servo-controlled universal testing machine was adopted. The vertical load was applied controlling the opening of a clip gauge located at the notch of the beam. Such measure is called Crack Mouth Opening Displacement (CMOD). The experimental curves obtained from five beams (in grey) are presented in Fig. 6 along with the mean curve (in black). The residual nominal tensile strengths of HPFRC were evaluated in accordance with EN 14651 [21]. Table 3 summarises the results obtained.

Table 3. Main HPFRC mechanical properties.

ID	$f_{cm,cube}$ [MPa]	E_{cm} [MPa]	f_{Lm} [MPa]	f_{R1m} [MPa]	f_{R2m} [MPa]	f_{R3m} [MPa]	f_{R4m} [MPa]
HPFRC	97.8 (0.06)	37828 (0.09)	8.61 (0.05)	13.63 (0.09)	12.63 (0.09)	11.06 (0.10)	9.41 (0.10)

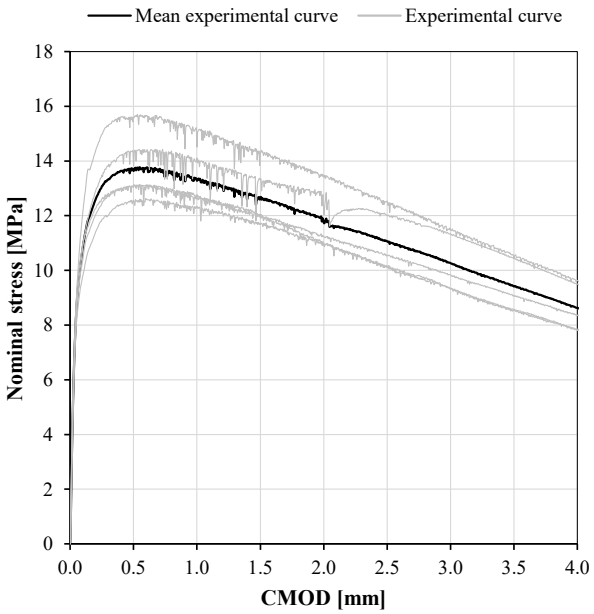

Fig. 6. Nominal stress vs. CMOD curves.

4 Results and discussion

4.1 Experimental results

The structural response of the specimens can be compared by means of the net deflection at the mid-span of the beam versus total load (see Fig. 7). At first glance, different responses in terms of stiffness, ultimate load and overall behaviour can be appreciated for Reference, Reinforced#01 and Reinforced#02 beams; details are given in Table 4.

Reference beams showed a similar response with an initial elastic branch with stiffness ranging between 318 kN/mm (specimen 01) and 423 kN/mm (specimen 02). The formation of first flexural cracks near the centre of the span was observed on average at 115 kN; after that, flexural stiffness started decreasing with an appreciable change in slope of the curve. Maximum vertical load was 394.2 kN (at 17.55 mm of deflection) for specimen 01 and 398.6 kN (at 13.37 mm of deflection) for specimen 02. Both the tests continued until failure due to longitudinal reinforcements rupture for a maximum displacement of 27.19 mm (corresponding to 345.9 kN) for specimen 01 and 340.2 kN (corresponding to 26.96 mm) for specimen 02. The final crack pattern of Reference-01 is shown in Fig.

8; it is characterized by several flexural cracks and few inclined cracks among which none can be considered a shear critical crack.

Experimental results on Reference beams confirmed a structural response dominated by a stut-and-tie resistance mechanism, in which the very low longitudinal reinforcement ratio caused the failure of the horizontal tie before the development of shear failure. It should be noted that, at the rupture of longitudinal reinforcement, the vertical legs of transverse reinforcements (lapped deformed bars) reached an average tensile stress of about 230 MPa. This tensile stress can be considered relevant since the transfer mechanism between the two bars (which form a closed hoop) relies only in the bond of the two u-shaped stirrups.

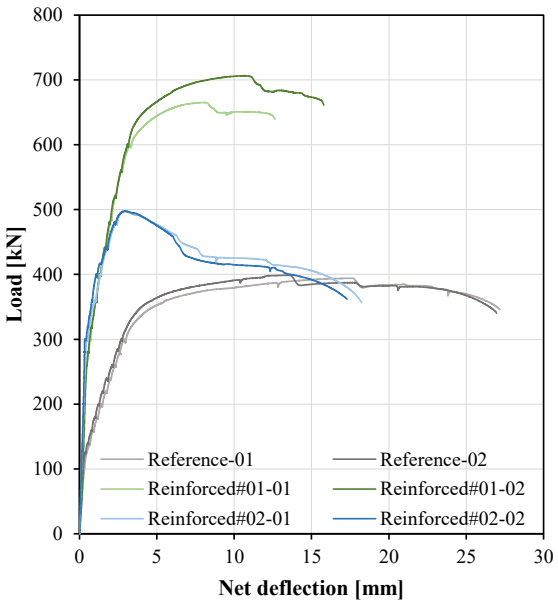

Fig. 7. Net deflection vs. load curves for the six beams tested.

Table 4. Main experimental results on beams in term of: maximum load (P_{max}), net deflection at maximum load $\delta(P_{max})$, ultimate load (P_u) and net deflection at ultimate load $\delta(P_u)$.

ID	P_{max} [kN]	$\delta(P_{max})$ [mm]	P_u [kN]	$\delta(P_u)$ [mm]
Ref.-01	394.2	17.55	345.9	27.19
Ref.-02	398.6	13.37	340.2	26.96
Reinfo.#01-01	665.1	8.11	639.0	12.62
Reinfo.#01-02	706.5	10.76	661.1	15.80
Reinfo.#02-01	498.2	2.87	357.0	18.25
Reinfo.#02-02	497.5	2.93	361.7	17.28

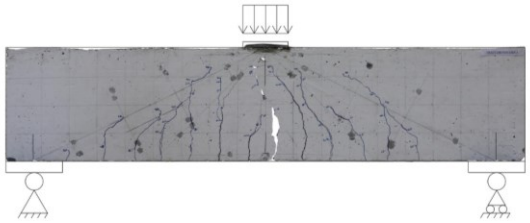

Fig. 8. Final crack pattern of Reference-01 specimen.

The test performed on Reinforced#01 beams showed a significant increase of the flexural stiffness and load-bearing capacity together with a reduction in ultimate displacement capacity. The flexural stiffness, measured on the elastic branch of the curve, was about 547 kN/mm (specimen 01) and 469 kN/mm (specimen 02). The first crack in the new HPFRC layer was observed around a load of 150 kN; after that, the slope of the curve has not changed significantly, due to due bridging capacity of fibres, able to transfer residual tensile stresses across cracks. Maximum vertical load was 665.1 kN (at 8.11 mm of deflection) for specimen 01 and 706.5 kN (at 10.76 mm of deflection) for specimen 02. Both the tests were completed after rupture of longitudinal reinforcements for a maximum displacement of 12.62 mm (corresponding to a load of 639.0 kN) for specimen 01 and 15.80 mm (corresponding to a load of 661.1 kN) for specimen 02. The resulting crack pattern was more complex than those of Reference beams due to the number of cracks developed during the test. The cracks were more numerous and smaller, with spacing below 50 mm. The jacketing with HPFRC and the addition of longitudinal reinforcements resulted in an average increase of the load bearing capacity of 73% and in an enhanced crack width control.

Reinforced#02 beams were reinforced with the HPFRC without any other reinforcement. Structural response was characterized by an increase of stiffness (+63 %) and an appreciable increase of load bearing capacity (+26%). After reaching the maximum load, the load-deflection curve in characterized by a descending branch until it reaches the maximum deformation. As in the previous cases, the specimens failed by rupture of the longitudinal reinforcements. Cracking occurred predominantly in the central portion of the beam (below the loading point) with spacing lower than 100 mm. The peculiar behaviour of the specimen is mainly influenced by the mechanical properties of HPFRC which has a tension softening behaviour. After reaching the maximum load, corresponding to the yielding of longitudinal bars, the load decreased due to the development of cracking process which is associated with the progressive opening of the cracks and the decrease of the residual tensile strength in HPFRC.

4.2 Displacement ductility factor

The displacement ductility factor, μ, is defined as the maximum displacement divided by the corresponding displacement when yielding occurs. This, simply defined in the following as ductility factor, was calculated for each specimen by considering five different analytical

models. The first is described in the ACI Guide 374.2R-13 [22]. The second, third and fourth refer to the work of R. Park concerning the evaluation of ductility of structures from laboratory testing [23]. The second and third are based on the principle of the equivalence of the ultimate displacement, while the fourth is based on the principle of equivalence of the displacement at maximum load. The fifth model is based on the principle of equivalence of the energies of the experimental curve and the bilinear curve used for the evaluation. The average values obtained in the calculation are summarised in Table 5.

Table 5. Ductility factor obtained by applying five different models.

	1st model	2nd model	3rd model	4th model	5th model
Ref.	8.86	9.35	7.44	4.24	10.02
Reinfo#01	6.82	5.29	4.67	3.10	5.82
Reinfo#02	27.78	38.28	14.11	2.11	20.99

Observing the experimental results in the light of the calculation of ductility factors, the following observations can be made:

- The first type of reinforcement (Reinforced#01 beams) is characterized by an increase in load-bearing capacity and a decrease in the deformation at yielding and a reduction in ultimate deformation. This information makes possible the evaluation of a general decrease in ductility factor according to all the models considered; with a reduction in ductility factor ranging between -23% and -43%.
- The second type of reinforcement (Reinforced#02 beams) provides encouraging results from this point of view. In fact, its response is characterised by an appreciable increase in load-bearing capacity, a noticeable reduction in yield deformation and a minor reduction in ultimate displacement capacity. These characteristics makes it possible to calculate a general increase in ductility factor according to all the models considered (with the exception of the 4th model), with the increase ranging between +90% and +310%.

5 Concluding remarks

Based on the tests performed and the results obtained, the following findings can be emphasized:

1. The first type of reinforcement (Reinforced#01 beams) increased the maximum and ultimate load of the original beam by 73% and 89%, respectively; but showed 48% lower ultimate displacements. The ductility factor decreased on average by 35% as compared to the original configuration of the beam before strengthening. This type of reinforcement has shown numerous micro-cracks at the end of the test.
2. The second type of reinforcement (Reinforced#02) has reached a maximum load increased by 26% as compared to the original state. The peak strength was reached for a very low displacement and deformation, but fracture toughness provided by fibres allowed to reach an ultimate displacement comparable to that assumed by the unreinforced beams. The evaluation of the ductility factor has given excellent results, improving up to 4 times with respect to the original state by considering the 2nd analytical model.
3. The amount of cracking developed was markedly different between the two types of reinforcement. The use of the fibres and additional reinforcements (Reinforced#01) generated a more diffused crack pattern with respect to that of the one observed in specimens without jacketing (Reference). In fact, the number of cracks was tripled as well as their length. With the second type of reinforcement (Reinforced#02), on the other hand, the crack pattern was similar to that of the specimens without jacketing. The fibres allowed a better control of the overall cracking; the crack opening was very limited when compared to beams without jacketing.
4. No problems related to delamination of the reinforcement around the core were found during the tests. The jacketing was perfectly adherent to the element to be reinforced even without the presence of connectors (Reinforced#02).

6 New challenges

In the coming years, the new challenge for the construction industry will be to reduce its environmental impact. Due to global warming, the construction industry is entering a new era in which every effort to reduce CO_2 emissions is necessary and can no longer be postponed. In this context, rehabilitation of reinforced concrete infrastructure with HPFRC could be a key tool because of the low amount of material to be used and the fewer number of construction phases needed on site. To assess the benefits in terms of CO_2 emissions, LCA analyses have already been conducted on such interventions, which have shown that the HPFRC intervention can reduce CO_2 emissions by more than 40 percent as compared to traditional reinforcement techniques.

Acknowledgments

The authors wish to express their gratitude and sincere appreciation to Italcementi HEIDELBERG Cement Group for supporting this research work. A special acknowledgement goes to Dr. Eng. Bruno Leporace, Eng. Michele Rossini, Mr. Augusto Botturi, Mr. Andrea Del Barba and Mr. Luca Martinelli for their support in carrying out the experimental project.

References

1 C. Andrade. *Initial steps of corrosion and oxide characteristics*. Str. Conc. 2020; **21**: 1710– 1719. https://doi.org/10.1002/suco.201900318.
2 C. Andrade, D. Izquierdo. *Propagation period modeling and limit state of degradation*. Str. Conc. 2020; **21**: 1720– 1731. https://doi.org/10.1002/suco.201900427.
3 P. Michael Enright, Dan M. Frangopol. *Probabilistic analysis of resistance degradation of reinforced concrete bridge beams under corrosion*. Eng. str. 20.11 (1998): 960-971.
4 P. Zampieri, M. A. Zanini, F. Faleschini. *Derivation of analytical seismic fragility functions for common masonry bridge types: methodology and application to real cases*. Engineering Failure Analysis, 2016, Vol. **68**, pp. 275-291, ISSN: 1350-6307, doi: 10.1016/j.engfailanal.2016.05.031.
5 M. A. Zanini, F. Faleschini, C. Pellegrino. *Bridge residual service-life prediction through Bayesian visual inspection and data updating*. Structure and Infrastructure Engineering, 2016, Vol. **13**, N. 7, pp. 906-917, ISSN: 1573-2479, doi: 10.1080/15732479.2016.1225311.
6 W. G. Buttlar, A. Chabot, E. V. Dave, C. Petit, G. Tebaldi. *Mechanisms of Cracking and Debonding in Asphalt and Composite Pavements*. State-of-the-Art of the RILEM TC 241-MCD; 2018, Springer - ISBN 978-3-319-76849-6.
7 A. Wargo, R. Y. Kim, W. Buttlar, B. Hill, G. Paulino, R. Roncella, A. Montepara, C. Petit, I. O. Pop, M. E. Kutay, E. Romeo, G. Tebaldi. *Digital image correlation techniques to investigate strain fields and cracking phenomena in asphalt materials*. Materials and Structures, 2014, doi.org/10.1617/s11527-014-0362-z.
8 M. M. Messore, L. Capacci, F. Biondini. *Life-cycle cost-based risk assessment of aging bridge networks*. Structure and Infrastructure Engineering, 2020, DOI: 10.1080/15732479.2020.1845752.
9 B. Belletti, F. Vecchi, C. Bandini, C. Andrade, J. S. Montero. *Numerical evaluation of the corrosion effects in prestressed concrete beams without shear reinforcement*. Str. Conc. 2020; **21**: 1794– 1809. https://doi.org/10.1002/suco.201900283.
10 M. A. Zanini, F. Faleschini, J. R. Casas Rius. *State-of-research on performance indicators for bridge quality control and management*. Frontiers in built environment, 2019, Vol. **5**, pp. 1-20. ISSN 2297-3362, doi: 10.3389/fbuil.2019.00022.
11 S. Campagnari, F. Di Matteo, S. Manzoni, M. Scaccabarozzi, M. Vanali. *Estimation of axial load in tie-rods using experimental and operational modal analysis.* Journal of Vibration and Acoustics, Transactions of the ASME, 2017. 139 (4), art. no. 041005, DOI: 10.1115/1.4036108.
12 A. Reggia, A. Morbi, G. A. Plizzari.. *Experimental study of a reinforced concrete bridge pier strengthened with HPFRC jacketing*. Eng. Str., Vol. **210** (2020), https://doi.org/10.1016/j.engstruct.2020.110355.
13 *fib* International Federation for Structural Concrete. *Model Code for Concrete Structures 2010*. Ernst & Sohn, ISBN 978-3-433-03061-5. 2013, p. 1–434.
14 F. Leonhardt, R. Walther. *Wardetiger Trager.* Deutscher Ausschuss fur Stahlbeton, Bulletin No. **178**, 1966, Wilhelm Ernst und Sohn , Berlin, German.
15 G.N.J. Kani. *Basic Facts Concerning Shear Failure*. Journal ACI, Vol. **63**, June 1966, pp. 675-692.
16 CEN European Committee for Standardization. *EN15630-1: Steel for the reinforcement and prestressing of concrete - Test methods - Part 1: Reinforcing bars, wire rod and wire*. Ed. by CEN. Brussels, Belgium, 2019.
17 CEN European Committee for Standardization. *EN12390-1: Testing hardened concrete - Part 1: Shape, dimensions and other requirements for specimens and moulds*. Ed. by CEN. Brussels, Belgium, 2021.
18 CEN European Committee for Standardization. *EN12390-2: Testing hardened concrete - Part 2: Making and curing specimens for strength tests*. Ed. by CEN. Brussels, Belgium, 2019.
19 CEN European Committee for Standardization. *EN12390-3: Testing hardened concrete - Part 3: Compressive strength of test specimens*. Ed. by CEN. Brussels, Belgium, 2019.
20 CEN European Committee for Standardization. *EN12390-13: Testing hardened concrete - Part 13: Determination of secant modulus of elasticity in compression*. Ed. by CEN. Brussels, Belgium, 2021.
21 CEN European Committee for Standardization. *EN14651: Test method for metallic fibre concrete - measuring the flexural tensile strength (limit of proportionally (LOP), residual)*. Ed. by CEN. Brussels, Belgium, 2005.
22 ACI American Concrete Institute. *ACI 374.2R-13 Guide for Testing Reinforced Concrete Structural Elements under Slowly Applied Simulated Seismic Loads*. Ed. by ACI, Farmington Hills, USA, 2013.
23 R. Park. *Evaluation of ductility of structures and structural assemblages from laboratory testing*. Bulletin of the New Zealand national society for earthquake engineering, Vol. **22**, No. 3, 1989.